Thermo-mechanical properties and creep modelling of wine lees filled Polyamide 11 (PA11) and Polybutylene succinate (PBS) bio-composites

Thermo-mechanical properties and creep modelling of Wine Lees filled Polyamide 11 (PA11) and Polybutylene succinate (PBS) bio-composites

A. Nanni, M. Messori

University of Modena and Reggio Emilia, Department of Engineering "Enzo Ferrari", Via Pietro Vivarelli 10/1, 41125 Modena, Italy

Solid wine wastes named wine lees (WL) have been mixed in different percentages (10, 20 and 40 phr) within Polyamide 11 (PA11) and Polybutylene Succinate (PBS) by twin-extrusion. Reactive extrusion has been also tested using 3-methacryloxypropyltrimethoxysilane tested as coupling agent. The obtained bio-composites have been characterized from a thermal (DSC, TGA, HDT), rheological (MFR), mechanical (tensile test) and thermo-mechanical (DMA, creep test) point of view. Micro-mechanics models of Voigt, Halpin-Tsai and Pukanszky have been fitted on tensile properties data meanwhile the creep behavior has been modeled and described through the models of Burger, Kohlrausch-Williams-Watts and Findley.

Keywords: Bio-composites; Thermo-mechanical properties; Creep modeling; Micro-mechanics

1. Introduction

In the last decades, because of the alarming plastic pollution [1] and the increasing oil price [2], polymers derived from renewable sources and/or biodegradable have gained a great attention in order to substitute the classical petrochemicals-derived and not degradable ones. Among them, Polyamide 11 (PA11) is a very attractive fully bio-based/non-biodegradable polymer. PA11 is obtained by condensation reactions of 11-aminoundecanoc acid that is generally derived from castor oil that, in its turn, is extracted from the *Ricinus Communis* plant [3]. It is characterized by a lower melting temperature if compared with other polyamides, has a good oil and water resistance, a fair biocompatibility, mechanical properties similar to polypropylene [4] and since its not biodegradability it is usually used for long-life applications as offshore flexible pipes and gas distribution pipes [5]. Similarly, Polybutylene succinate (PBS) represents one of the most promising

biodegradable polymer because its excellent ductility and melt processing capability which makes it suitable for many fields as flexible packaging, agriculture and consumers goods. PBS is a polyester synthesized by poly-condensation of 1,4-butanediol and succinic acid. Until recently, both PBS monomers have been generally obtained through several reactions starting from petrochemicals products (e.g. oxygenation of butane to maleic anhydride that hydrated forms maleic acid that yields succinic acid through hydrogenation or BASF's Reppe reactions to produce 1,4-butandiol). Nowadays, these monomers have started to be obtained also trough fermentation of agro-industrial wastes or other renewable sources [6-8], and the biomass-derived content of PBS is estimated to represent the 80% [9]. Despite these potentials, in 2018 the production of bio-based/non-biodegradable and biodegradable polymers has been of 1.2 Mt (millions of tons) and 0.91 Mt, respectively, representing only the 0.35% and 0.26% of the total global polymer production [10, 11]. This limited presence in the market has been due to the bio-based and/or biodegradable polymers prices, still significantly higher than petrochemicals ones. To decrease biopolymers costs, different attempts to exploit agro-wastes within the plastic word as fillers [12-15] or additives [16-18] have been carried out in the recent past. In the present work, the wine lees (WL), by-products formed after fermentation as residues obtained by filtration or centrifugation of wines have been tested in different percentage as natural cost-advantage filler within PA11 and PBS. WL are mainly composed by died microorganisms, lignin, proteins, organic salts, carbohydrates and important inorganic fractions due to the use of bentonite clay during the winemaking flocculation and clarifications steps [19]. WL have been selected because their yearly huge amount generation (2 Mt worldwide and 0.4 Mt only in Italy [20]), their reinforcement effect exhibited within other biopolymers [15] and their cost-effectiveness (0.045 €/kg [21]).

2. Material and methods

2.1. Materials

Polyamide 11 (PA11) – typology "Rilsan ® BMNO" (melting temperature = 189 °C, density = 1.03 g cm^{-3}) – has been supplied by Arkema (Paris, France) meanwhile poly(butylene succinate) (PBS) – typology PBE 003 (melting temperature = 115 °C, density = 1.26 g cm^{-3}) - has been supplied by NaturePlast (Caen, France).

The wine lees (WL) have been obtained from the winery Cevico Group C.V.C (Lugo (RA), Italy) in 2018 September by raking after alcoholic fermentation of red Sangiovese grapes.

3-Methacryloxypropyltrimethoxysilane GENIOSIL® GF31 (sil) and the paraffinic oil "Vestan" have been provided by Wacker Chemie AG (München, Germany) and Tizi, S.R.L (Arezzo, Italy), respectively.

2.2. Preparation of the PA11 and PBS-based materials

PA11 and PBS pellets have been mixed with different contents of WL (10, 20 and 40 phr) by the means of a laboratory twin-screw extruder Haake Rheomex 557. Reactive extrusion has been also tested adding 1 phr of sil to the formulation containing 20 phr of WL. In other cases, 1 phr of sticky Vestan oil has been used to enhance adhesion between WL and pellet surfaces before extrusion. Polymers and WL have been oven-dried at 80 °C for 4 hours to remove eventual absorbed moisture before this step. The extruded filaments have been air-cooled, manually spooled and grounded. The compounded pellets have been fed in a Tecnica DueBi MegaTech H10/18-1 injection-molding machine to obtain tensile test specimens (type 1BA, ISO 527) and rectangular specimens for dynamic-mechanical analysis, creep and heat distorsion temperature tests. The composition of each investigated formulation is reported in Table 1, meanwhile processing conditions are available in supplementary data.

Table 1
Codes and compositions of the investigated materials.

PA11-based samples	Composition	PBS-based samples
PA11 proc	Neat polymer processed in the same conditions	PBS proc
PA11 10WL	Polymer + 1 phr Vestan + 10 phr WL	PBS 10WL
PA11 20WL	Polymer + 1 phr Vestan + 20 phr WL	PBS 20WL

PA11 40WL	Polymer + 1 phr Vestan + 40 phr WL	PBS 40WL
PA11 20WL sil	Polymer + 20 phr WL + 1 phr sil	PBS 20WL sil

2.3. Wine lees characterization

The WL used in this work have been the same used in a previous work [15], where moisture content, density, particle size distribution, organic and inorganic fractions (by muffle-furnace), morphology and elementary composition are reported. To extend the WL characterization, thermogravimetric analysis (TGA) and FT-IR spectra have been reported and discussed in the present work. WL powder FT-IR spectra have been collected using a Perkin-Elmer Spectrum GX Infrared Spectrometer. Spectra have been obtained in ATR mode as an average of 64 scans in the 4000-400 cm^{-1} range with a 4 cm^{-1} resolution. TGA conditions have been the same of the ones reported in paragraph 2.4.3.

2.4 PA11 and PBS-based materials characterization

2.4.1. Differential Scanning Calorimetry (DSC)

Thermal properties of PA11 and PBS-based samples have been evaluated by Differential Scanning Calorimetry (DSC) (DSC TA 2010), using 7 ± 2 mg of sample and purging the chamber with 50 mL min^{-1} of nitrogen. Each sample has been firstly heated from 25 to 230 °C at 20 °C min^{-1} (PA11-based materials) [from 25 to 180 °C at 15 °C min^{-1} (PBS-based materials)] to erase previous thermal history and subsequently cooled to -30 °C at 15 °C min^{-1} (PA11-based materials) [to -40 °C at 10 °C min^{-1} (PBS-based materials)]. Finally, samples have been heated again to 230 °C at 15 °C min^{-1} (PA11-based materials) [to 180 °C at 10 °C min^{-1} (PBS-based materials)]. Crystallization temperature (T_C) and enthalpy (H_C) have been collected from the cooling cycle, meanwhile melting temperature (T_m) and enthalpy (H_m) and, when detectable, glass transition temperature (T_g) have been carried out from second heating cycle. Melting enthalpies have been calculated considering the additives and fillers weight fractions. Crystallinity percentages (% Cr) have been obtained using the values of 206 J g^{-1} [22] and 110 J g^{-1} [23] as PA11 and PBS reference melting enthalpies values, respectively.

2.4.2. Melt Flow Rate (MFR)

Melt mass flow rate (MFR) has been determined according to ISO 1133 (part II, materials sensitive to moisture) with a load of 2.16 kg and a temperature of 235 °C for PA11-based samples and 190 °C for PBS-based ones.

2.4.3. Thermogravimetric Analysis

TGA has been conducted on 15 ± 5 mg of sample by the means of TG-NETZSCH STA 409 using a ramp temperature of 10 °C min^{-1} from 25 °C to 600 °C and purging the chamber by 50 mL min^{-1} of air. Temperatures at 5%, 10% and 15% weight loss (T_5, T_{10} and T_{15}, respectively) as well as the residue at 600 °C (Res_{600}) have been measured from the thermograms.

2.4.4. Tensile tests

Tensile tests have been performed using the INSTRON 5567 dynamometer equipped with a 1 kN load cell and a 25 mm gauge length extensimeter. Tests have been conducted with a clamp separation speed of 10 mm min^{-1} for the PA11-based samples and of 20 mm min^{-1} for the PBS-based ones. Young's modulus (E), tensile strength (σ_M) and elongation at break (ε_b) have been measured and reported for each formulation as average of at least six determinations. The micro-mechanics models for composites of Voigt [24] and Halpin-Tsai [25] have been exploited to extrapolate the Young's modulus of WL particles (E_P). Similarly, Pukanszky's equation has been used on tensile strength data to extrapolate the empirical adhesion B factor [26]. The mentioned model equations are reported as follow:

$$Voigt: E_C = E_P V_P + E_M(1 - V_P)\ (Eq.1)$$

$$Halpin - Tsai: E_C = E_M \frac{1 + 2\eta V_P}{1 - \eta V_P}\ (Eq.2)\ with\ \eta = \frac{E_P/E_M - 1}{E_P/E_M + 2}$$

$$Pukanszky:\ \sigma_C = \sigma_M \frac{1 - V_P}{1 + 2.5V_P} \exp(BV_P)\ (Eq.3)$$

where E_C is the composite modulus, E_M is the polymer matrix modulus, E_P is the filler particle modulus, V_P is the filler particle volume fraction and B is the Pukanszky's empirical adhesion constant.

2.4.5. Dynamic Mechanical Analysis

TA DMA Q800 instrument has been used in single cantilever configuration to evaluate the dynamic mechanical behavior of PA11 and PBS-based samples. Tests have been run from -40 °C to 80 °C with a heating rate of 3 °C min^{-1}, an oscillating frequency of 1 Hz and an applied strain of 0.1%. Glass transition temperatures (T_g) values have been recorded as the maximum values of the tanδ curves.

2.4.6. Creep tests

Creep properties have been measured at 20, 40, 60 and 80 °C using the TA DMA Q800. Creep compliance has been recorded loading the specimens with a 1 MPa stress for 10 min. The experimental data have been fitted with the micromechanical models of Burger, Kohlrausch–Williams–Watts (KWW) and Findley in order to extrapolate and model useful information on the creep behavior of the tested samples. First attempt values have been assigned to the model's parameters and subsequently they have been optimized minimizing the difference between empirical and theoretical values and imposing the coefficient of determination (R^2) equal to one.

2.4.7. Heat Distortion Temperature

The heat distortion temperature (HDT) of the PA11 and PBS-based samples have been carried out adapting the ASTM International Standard D 648 on the DMA Q800 as here described [27]. Rectangular specimens (5 mm of width and 2 mm of thickness) have been placed on the tree-point bending clamps (50 mm of length) and stress of 0.455 MPa has been applied raising the temperature from 25 °C at 2 °C min^{-1}. HDT has been recorded as the temperature at which the test bar has deflected by 0.25 mm.

2.4.8. Scanning Electron Microscope

Specimens have been broken in liquid nitrogen and cross section covered by a 10 nm thickness gold layer. The treated surface have been observed with an environmental Scanning Electron Microscope ESEM Quanta FEI 2000 operating in low-vacuum conditions and equipped with a microanalysis X-EDS Oxford INCA-350 syestm.

3. Results and discussion

3.1 Wine Lees characterization

The high inorganic fraction of WL has been confirmed by the thermogravimetric analysis (Fig.1) that has reported a WL Res_{600} value of nearly 40%, in perfect accordance with the not-volatile fractions evaluated by muffle-furnace test in a previous work [15]. The organic fraction has started to thermally degrade in one step at 257 °C (T_5) and already at 267 °C (T_{15}) the 15% of the mass weight was lost. Despite this very fast weight loss, is appreciable that WL degradation has begun at temperatures higher than PBS and PA11 processing ones.

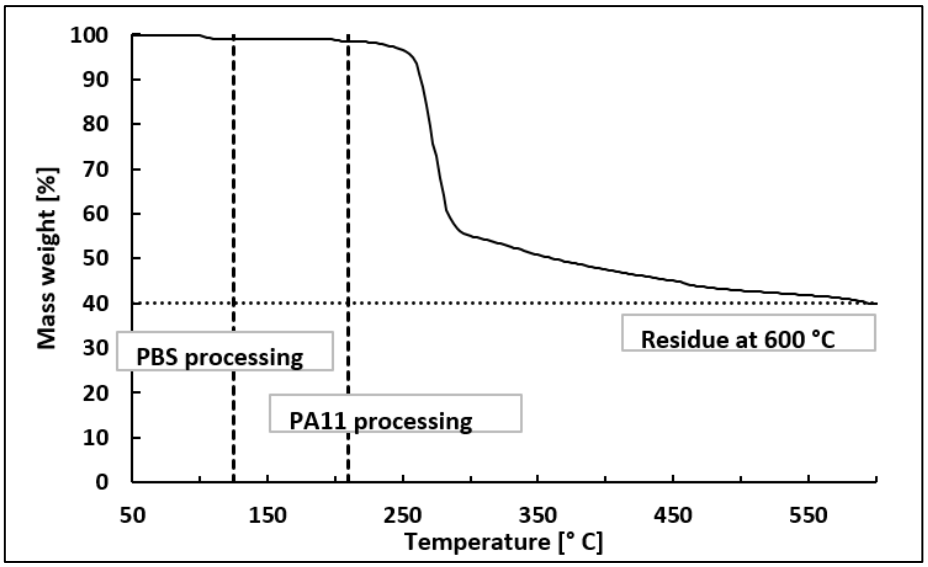

Fig.1 TGA curve of WL under air gas flow.

The organic fraction of WL has been confirmed to be composed mainly by yeast (peaks b, e, f, g, h and i), tartaric acid and their derivate (peaks a, d and i), carbohydrates (peaks h and i) and traces of lipids derived by the grape seeds (peaks c and d), as shown by FT-ATR analysis (Fig.2 and Table 2).

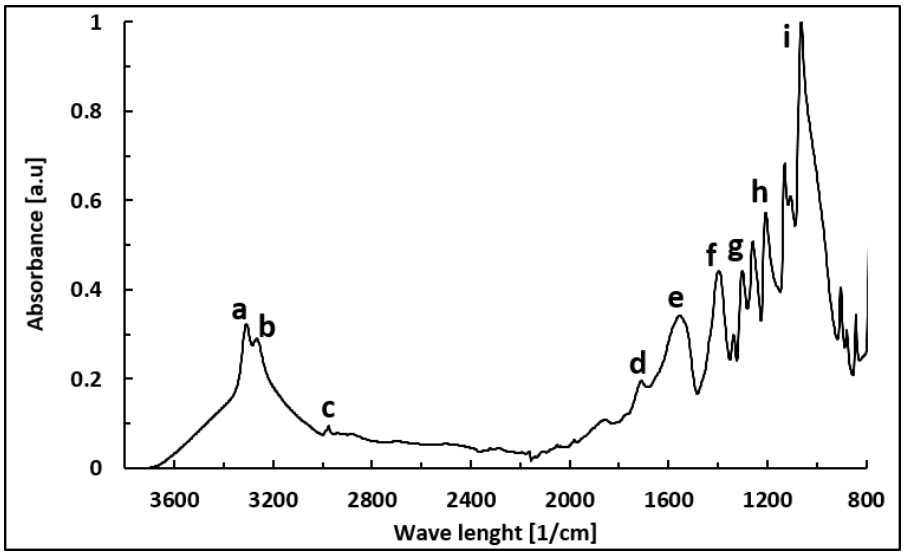

Fig.2 FT-IR ATR spectrum of the WL.

Table 2
WL FT-IR ATR spectrum: absorption peaks and corresponding assignments.

Peak code	Wave number [cm^{-1}]	Assignment
a	~ 3400	O-H and N-H stretching vibration of polysaccharides and tartaric acid
b	~ 3300	N-H stretching of proteins and peptides
c	~ 2920	Asymmetric stretching vibration of CH2 lipids (Hydrocarbon tails)
d	~ 1740	C=O stretching in lipid esters and in tartaric acid
e	~ 1550	Amide II: N–H and C–N vibrations of the peptide bond in different protein conformations
f	~ 1390	CO of COO^- symmetric stretching in proteins
g	~ 1300	Amide III: C–N and C–O stretching, N–H and OC–N bending
h	~ 1210	C–O stretching free nucleotides/ C–O–C carbohydrates
i	~ 1160	C-C, C-O and C-N stretching vibrations

3.2 Thermal properties and Melt Flow Rate

The main thermal properties and the MFR values of the investigated composites have been reported in Table 3. No significant differences in thermal behavior of both PA11 and PBS-based samples have been found by adding WL as filler. Crystallinity has been improved using 20 phr of WL (+10.9% in PA11 20WL and +17.7% in PBS 20WL) pointing out the WL possibility to partially work as nucleating agent [28]. This property has disappeared using 40 phr of WL because of probable agglomeration phenomena of WL particles.

Table 3
PA11 and PBS-based samples thermal properties.

Sample code	MFR [g/10']	T_C [° C]	H_C [J g^{-1}]	T_g [° C]	T_m [° C]	H_m [J g^{-1}]	% Cr
PA11 Proc	19 ± 1	159	43	51	189	49	23.8
PA11 10 WL	15 ± 0	161	40	49	189	46	24.8
PA11 20 WL	12 ± 0	161	42	50	189	45	26.4
PA11 40 WL	11 ± 0	160	29	48	190	32	21.9
PA11 20 WL sil	8 ± 0	161	37	48	189	40	23.5
PBS Proc	8 ± 0	89	71	-	115	69	62.1
PBS 10 WL	8 ± 0	87	65	-	115	65	65.4
PBS 20 WL	11 ± 1	86	69	-	115	67	73.1
PBS 40 WL	9 ± 1	83	53	-	115	55	70.2
PBS 20 WL sil	7 ± 0	85	57	-	116	59	64.9

Finally, WL have slightly increased the viscosity of PA11-based samples as shown by MFR values, similarly to other works on composites. Nevertheless, the increased viscosity has not been enough to affect the injection molding processability. On the other hand, PBS-based samples MFR values have not been significantly modified by the WL particles remaining close to the PBS proc ones.

3.3 Mechanical and thermo-mechanical properties

3.3.1 Tensile test

Table 4
PA11 and PBS-based samples tensile properties.

Sample code	E [MPa]	ΔE [%]	σ_M [MPa]	$\Delta\sigma_M$ [%]	ε_b [%]	$\Delta\varepsilon_b$ [%]
PA11 proc	1113 ± 57	-	33.8 ± 2.6	-	305 ± 26	-
PA11 10 WL	1200 ± 42	+ 7.9	28.3 ± 2.2	- 16.2	227 ± 36	- 25.6
PA11 20 WL	1318 ± 78	+ 18.5	26.1 ± 3.8	- 22.8	167 ± 30	- 45.2
PA11 40 WL	1494 ± 65	+ 34.3	24.7 ± 1.0	- 26.9	47.8 ± 4.5	- 84.7
PA11 20 WL sil	1260 ± 51	+ 13.2	26.5 ± 0.6	- 21.6	177 ± 16	- 42.1
PBS proc	683 ± 28	-	32.7 ± 2.1	-	394 ± 24	-
PBS 10 WL	775 ± 12	+ 13.5	28.9 ± 1.1	- 11.6	286 ± 41	-27.4
PBS 20 WL	865 ± 26	+ 26.6	23.6 ± 0.7	- 27.8	188 ± 43	- 52.3
PBS 40 WL	946 ± 30	+ 38.5	21.3 ± 1.8	- 34.9	50.2 ± 12.9	- 87.2
PBS 20 WL sil	834 ± 23	+ 22.2	24.8 ± 0.6	- 24.1	151 ± 54	- 61.7

The tensile properties of PA11 and PBS-based samples are reported in Table 4. It is possible to notice a WL stiffening effect on both polymeric matrices. Young modulus (E) has been linearly increased with the WL content and this fact has denoted a good dispersion of the particles inside the matrix. In particular, PA11 40WL and PBS 40WL samples have respectively shown enhanced elastic moduli of

nearly + 34% and + 39% if compared to neat polymers. The gain in Young modulus has been explained by the higher intrinsic stiffness of WL particles rather than polymer matrices due to their high inorganic fractions. As example, Aluminum silicates and Potassium tartrates found out within PBS 20WL sample have been reported in Fig 3. The WL elastic modulus (E_P), quantified fitting Voigt and Halpin-Tsai models on experimental data has been calculated to lie between 2.2 and 3.2 GPa (Table 5). In this work, WL elastic modulus seems inferior to the one extrapolated previously [15], but in this case E_P values are more convergent (especially considering Halpin-Tsai model).

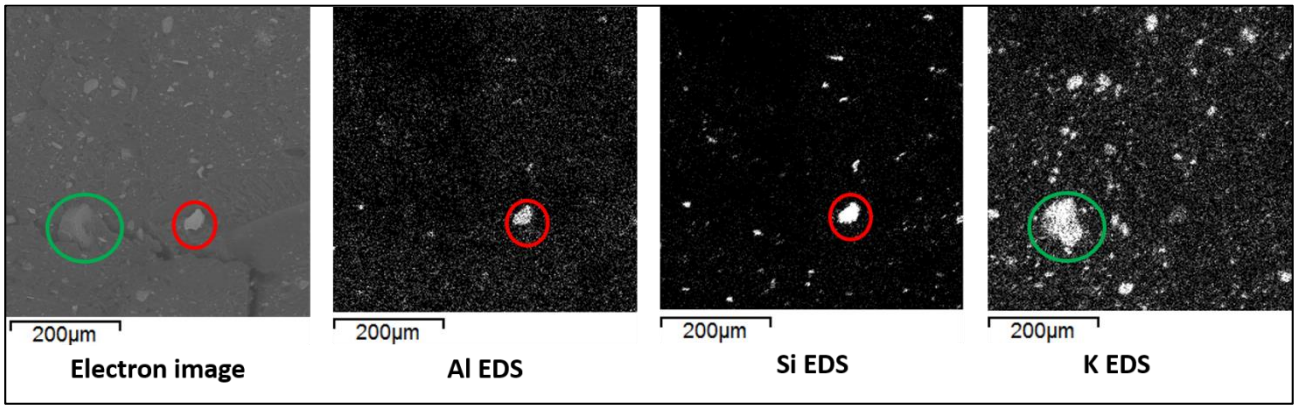

Fig.3 SEM image of PBS 20WL and overlap of Al, Si and K EDS revelations. Green circle refers to Potassium tartrates meanwhile red circle to Alumina silicates.

The tensile strength has been decreased increasing the WL content in both PA11 and PBS-based samples. In composites, this mechanical property is strongly affected by the particle-matrix adhesion. Poorly bonded particles are not able to transfer the stress trough the interface; thus discontinuities and de-wetting phenomena are generated and crazes formation happens earlier and for low applied stresses than with well-bonded particles [29, 30]. The Pukanzsky's B adhesions factors is an empirical constant able to quantify the particles-matrix adhesion. It tends to zero for poorly bonded particle meanwhile raises up progressively with the increasing of the particle-matrix interactions. In this case, because of polymers hydrophobicity and WL hydrophilicity, B factors have not been too great if compared to other works [15, 31, 32], but neither too bad, being higher than zero (Table 5).

Table 5

Micro-mechanics: WL elastic moduli (E_P) evaluated through both Voigt and Halpin-Tsai models and empirical B adhesion factor from Pukanszky's equation.

E_P [MPa] using Voigt Model					
	10 WL	20 WL	40 WL	20 WL sil	Average
PA11-based	2416	2744	2817	2283	2565 ± 222
PBS-based	1874	1948	1730	1735	1822 ± 93
E_P [MPa] using Halpin-Tsai Model					
	10 WL	20 WL	40 WL	20 WL sil	Average
PA11-based	3162	3960	3936	2801	3465 ± 500
PBS-based	3252	3371	2379	2562	2891 ± 428
Pukanszky's B adhesion factor					
	10 WL	20 WL	40 WL	Average	20 WL sil
PA11-based	0.71	1.18	1.72	1.20 ± 0.41	1.31
PBS-based	1.73	0.95	1.39	1.35 ± 0.39	1.29

Tensile strength has been drastically reduced using 10 WL phr, and subsequently, with 20 and 40 WL phr, a smaller reduction tending to an asymptote has been observed (Fig.4). This can be explained by the fact that at low particle's loadings, fillers are not well dispersed in the matrix and create high stress concentrations spots that break the particle-matrix bonds [33]. Finally, the not significant enhancement of the tensile strength values of samples containing silane has pointed out the inefficiency of the reactive extrusion for these bio-composites.

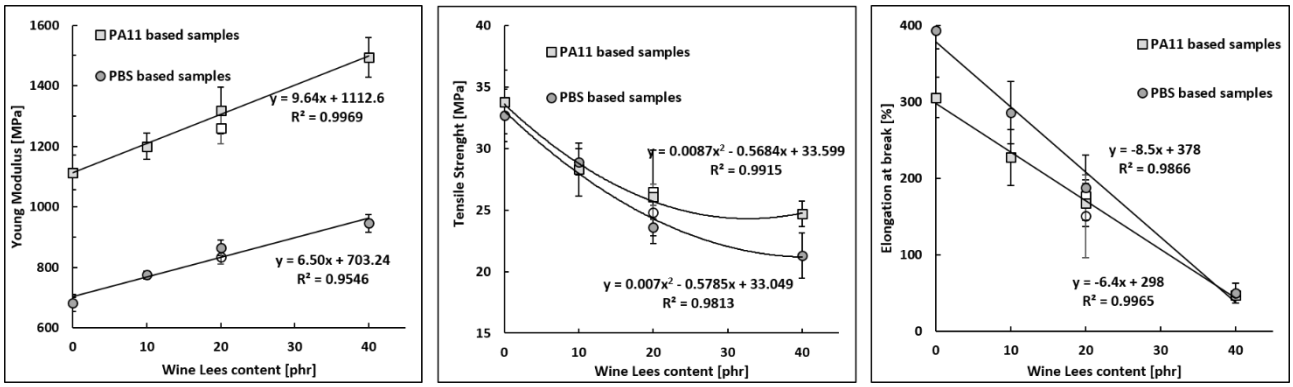

Fig.4 Young modulus, tensile strength and elongation at break as WL content function for PA11 and PBS-based samples. Unfilled symbols refer to containing silane formulations.

As expectable, the elongation at break (ε_b) of neat polymers have been decreased by WL concentration as often reported [29, 34]. Nevertheless, it is noteworthy underline that also with high particles loadings significant elongation at break values have been maintained (167% in PA11 20WL and 188% in PBS 20WL) if compared with other PA11 and PBS-based composites (Table 6). Small

decreases in ductility can be due to both partial plasticization effects and good miscibility between WL and polymers that not completely decrease the chain mobility [35, 36]. The possibility of a partial plasticization induced by WL on matrices is also supported by the lower T_g values carried out in filled polymers (Tables 3 and 7).

Table 6
Elongation at break (ε_b) values of different PA11 and PBS composites reported in literature.

Matrix	Filler charge and typology	ε_b [%]	Test speed (mm min^{-1})	Ref
PA11	20%wt. stone ground-wood fibers	9.5±0.8	2	[37]
PA11	15%vol. PHB whisker	8±3	1	[38]
PA11	25%wt. lignin	9±2	1	[35]
PBS	20%wt modified jute fibers	3±2	5	[39]
PBS	30%wt lignin	4.6±0.3	Not specified	[40]
PBS	10%wt Oil Palm Mesocarp Fibers	19.6±2.9	5	[33]

3.3.1 Dynamic Mechanical Analysis

Table 7
Storage moduli E' at different temperatures (0, 25, 50 and 75 °C), T_g (max tanδ) and interpolating equation of PA11 and PBS-based samples.

E'(T) [MPa]	PA11 proc	10 WL	20 WL	40 WL	20 WL sil	Interpolating equation*
E'(0)	1178	1354	1412	1602	1448	y=10.1x + 1210 R^2=0.967
E'(25)	1111	1255	1301	1489	1335	y=9.0x + 1131 R^2=0.977
E'(50)	842	849	892	1079	928	y=6.2x + 808 R^2=0.898
E'(75)	342	333	364	459	353	y=3.2x + 319 R^2=0.866
T_g [°C]	66.2	64.2	62.6	63.9	63.7	
E'(T) [MPa]	PBS proc	10 WL	20 WL	40 WL	20 WL sil	Interpolating equation*
E'(0)	888	1026	1178	1293	1131	y=10.1x + 920 R^2=0.945
E'(25)	629	719	831	920	798	y=7.3x + 647 R^2=0.956
E'(50)	474	553	635	700	613	y=5.6x + 493 R^2=0.946
E'(75)	318	385	442	482	421	y=4.0x + 337 R^2=0.916
T_g [°C]	-20.2	-19.3	-19.3	-20.0	-19.6	

* Storage modulus (y) as WL content expressed in phr function (x).

The storage moduli (E') of PA11 and PBS-based samples have been reported as temperature's function in Fig.5 as well as in Table 7. The WL stiffening effect has been confirmed within the whole range of tested temperatures appearing more markedly below T_g, but still appreciable at 75 °C where the use of 40 phr of WL has guaranteed E' values 1.3 and 1.5 higher than PA11 proc and PBS proc, respectively. T_g has been confirmed to be lowered by WL fillers in both PA11 and PBS-based samples, similarly to what noticed in DSC measurements (only for PA11). The presence of a single

T_g (one tanδ peak) confirms also the existence of a single phase system with good miscibility [35, 41].

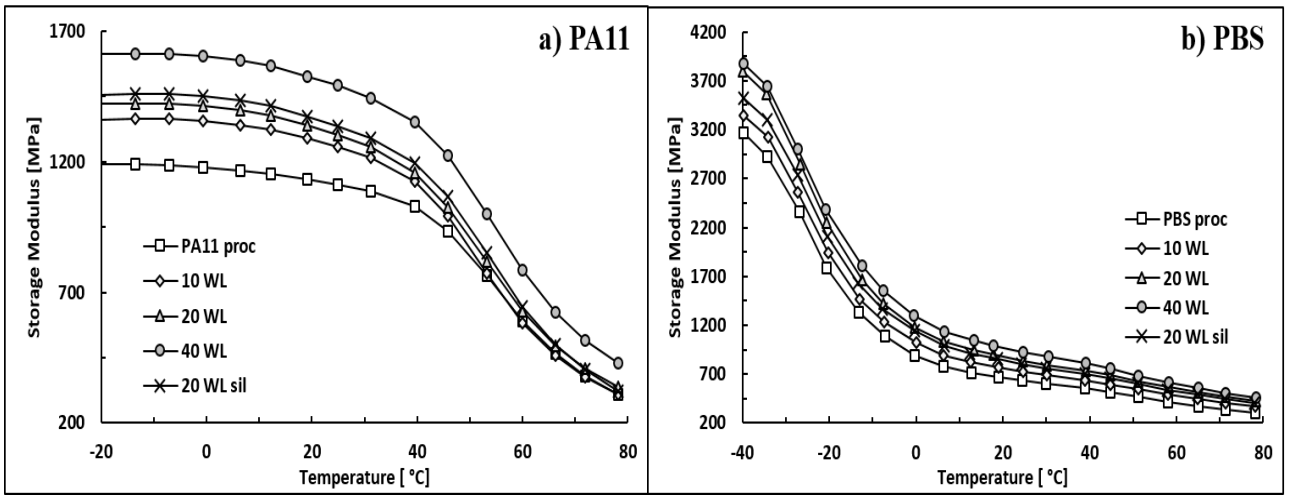

Fig.5 Storage modulus of (a) PA11and (b) PBS-based samples as a function of temperature.

The interpolating equations reported in Table 7 (E' as a function of WL) point out that storage modulus has been linearly increased by WL, similarly to what observed in other works regarding WL composites. Therefore, plotting all these data (Fig.6), it has been possible carry out a correlation formula suitable for the prediction of the storage modulus of WL filled bio-polymers at a certain temperature. The mentioned equation has the following form:

$$\frac{E'_C(T)}{E'_M(T)}(WL) = 1 + 0.01WL \ (Eq.4)$$

where $E'_M(T)$ is the storage modulus of the neat polymer at temperature T, $E'_C(T)$ is the storage modulus of the WL filled composite at temperature T, and *WL* is the wine lees content expressed in phr.

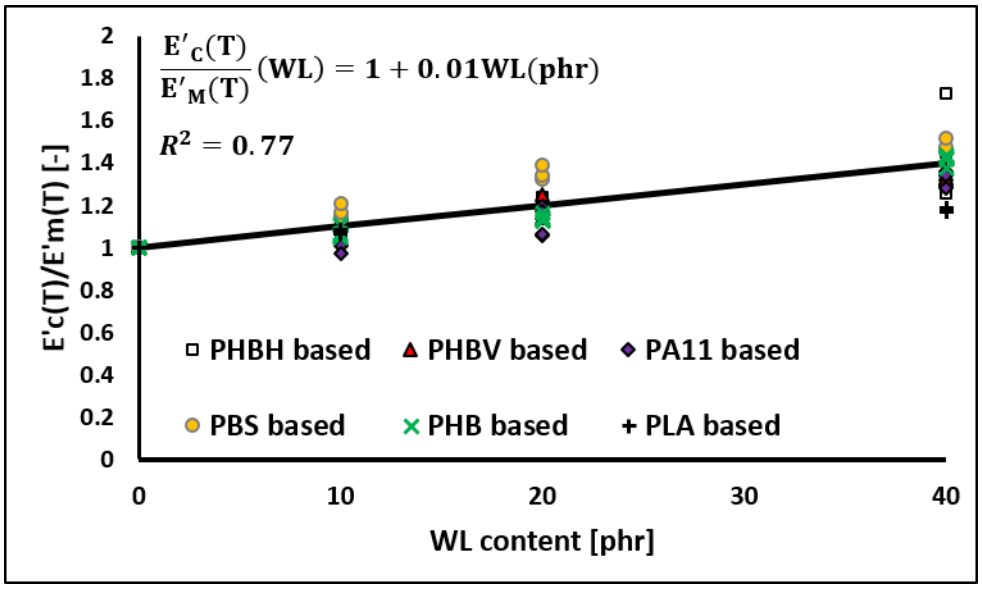

Fig.6 Storage moduli of several WL filled bio-composites and proposed predictive curve.

3.3.2 Modeling of the creep behavior

The creep compliance curves at different temperatures of PA11 and PBS-based samples have been reported in Fig.7, where is possible to notice how WL have been able to significantly increase the creep resistance. The creep resistance gap between neat polymers and composites has become greater especially for high particles loadings (40WL phr) and for high temperatures (60 and 80 °C). From an applicative point of view, this mechanical enhancement is particularly useful for PA11-based composites that are often applied for long-life applications [42] since their not biodegradability.

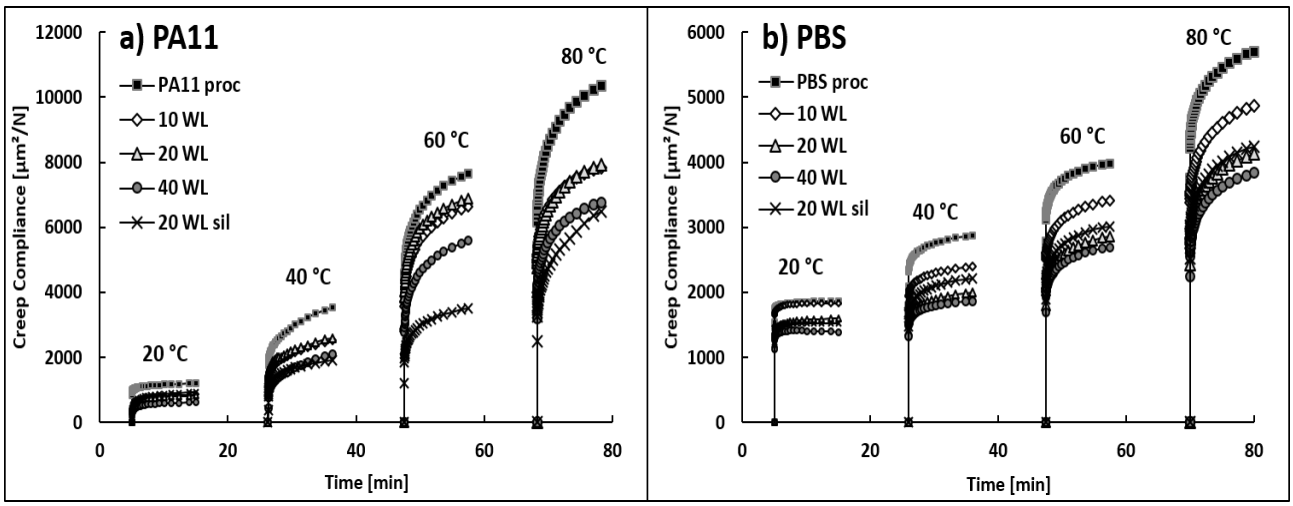

Fig.7 Creep compliance curves for PA11 and PBS-based samples at 20, 40, 60 and 80 °C.

Generally, the trend of the isothermal creep compliance can be described by three different components: a pure elastic component, a viscoelastic component and a plastic irreversible component [43]. In this work, no plastic deformations have been produced since total recovery of the initial length has been observed after unloading. Therefore, to evaluate the effects of WL on the elastic and viscoelastic components of the creep response three different micro-mechanics theoretical creep models have been fitted on experimental data. Burgers model [44] is based on a four-element mechanical system composed by the combination of Maxwell series and Kelvin elements and it has been successfully applied for creep data analysis of various semi-crystalline polymers [45]. The creep compliance formula of this model is given by:

$$J(t) = \frac{1}{E_M} + \frac{1}{\eta_M} + \frac{1}{\eta_K}\left[1 - exp\left(-\frac{E_K}{\eta_K}t\right)\right] \quad (Eq.5)$$

where E_M and η_M are the elastic and viscous parameters of the Maxwell series elements, meanwhile E_K and η_K are the elastic and viscous parameters of the Kelvin parallel elements. Another successful model applied to creep data of glassy solids [46] and semi-crystalline polymers [47] is the Kohlrausch-Williams-Watts (KWW) model. KWW model derives from the consideration that viscoelastic changes in polymeric matrices occur because of molecular incremental jumps due to several segments chains jumps between different positions of relative stability [48]. The KWW model describes the creep compliance through a four parameters Weibull-like function and its formula is given by:

$$J(t) = J_i + J_c\left\{1 - exp\left[-\left(\frac{t}{t_c}\right)^{\beta_c}\right]\right\} \quad (Eq.6)$$

where J_i is the instantaneous elastic creep compliance component, J_c is the limit viscous creep compliance value and t_c and β_c are the scale (characteristic time) and shape parameters, respectively. Expanding the KWW function as a series and ignoring all terms except the first one is possible to obtain a power law consistent with Findley's equation [49], here reported:

$$J(t) = J_i + kt^n \ (Eq.7)$$

where J_i is again the elastic instantaneous creep compliance contribute, k is a coefficient related to the underlying retardation process and n is an exponent taking into account the time dependence of creep response. As an example, in Fig.8 creep data of PA11 proc, PA11 10WL and PA11 40WL at 40 °C as well as PBS proc, PBS 10WL and PBS 40WL at 60°C have been fitted by Burgers and KWW equations, meanwhile all extrapolated parameters are available in Supplementary data.

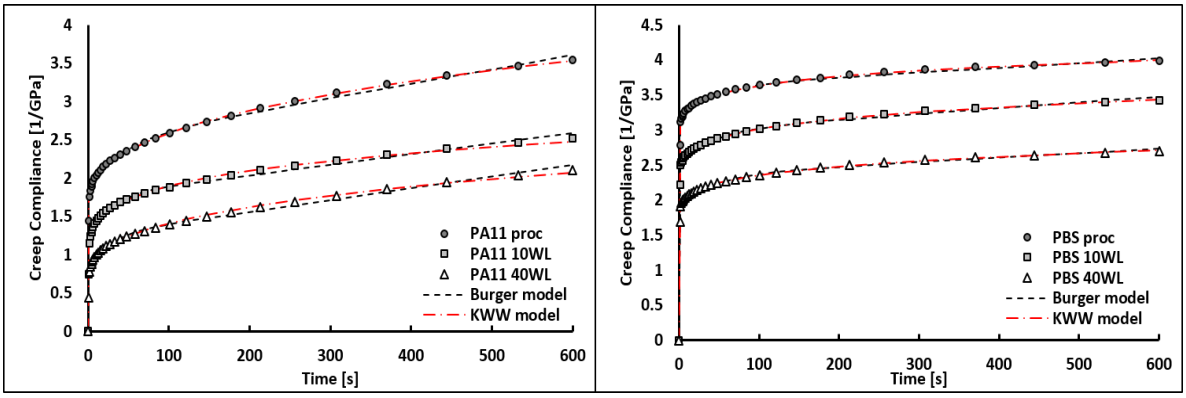

Fig.8 Creep compliance data of some PA11-based samples at 40 °C and some PBS-based samples at 60° C and fitting Burger and KWW models curves.

In Fig.8, it is possible to observe that for PA11-based samples Burger model is only partially able to fit the experimental curve because at longer times a linear increase in creep compliance caused by the Maxwell dashpot element (η_M) contribution is observable. Physically, the creep deformation associated with this element is irreversible after unloading and this fact is in contrast with this experiment as before mentioned. Further, according to Burger model, the creep compliance reduction should have been reflected by an increasing of both elastic (E_M, η_M) and viscous parameters (E_K, η_K) and this has occurred in most of both PA11 and PBS-based samples cases. Considering KWW parameters, it is possible to state that elastic creep contribute (J_i) have been decreased by the WL particles in both PA11 and PBS-based samples and for each temperature, in perfect agreement with the WL stiffening effect revealed by tensile test and DMA. Similarly, the viscous creep compliance with time tending to infinite ($J_i + J_c$) has been found to be reduced in almost each tested sample and temperature (-27% in PA11-based samples and -14% in PBS-based samples, on average) confirming

the WL ability to decrease the creep extent as carried out in previous work [15]. Nevertheless, contrarily to PHBH and PHBV-WL based samples [15], t_c has been reduced by the WL adding in both polymer matrices. This means that bio-composites deform more rapidly than neat polymers but to a lower extent. Concluding, each investigated model has led to the same physical creep behavior interpretation. KWW and Findley's models have been able to excellently fit both PA11 and PBS-based samples experimental data meanwhile Burger's model should not be used to describe PA11-based samples compliances data.

3.3.3 Heat Distortion Temperature (HDT) and Thermogravimetric Analysis (TGA)

Heat Distortion Temperature (HDT) is a key parameter for the identification of the maximum service temperature for a plastic product. HDT values of PA11 and PBS-based samples have been reported in Table 8. It is possible to notice that WL have enhanced this property of nearly 10% and 17% if compared with neat PA11 and PBS, respectively. This improvement is a consequence of the WL stiffening effect caused by the hindering of segmental polymer chains that makes materials more resistant to deflection [50, 51]. Despite this enhancement, it is noteworthy underline that TGA curves (Fig.5) have been significantly shifted to lower temperatures. The thermal degradation behavior has been the same for all samples as confirmed by the identical TGA curves shape, but WL filled samples have started to loose weight much earlier (T_{10} reduction of nearly -80 °C and -35 °C comparing respectively PA11 and PBS-filled samples with neat polymers). This has been due by the intrinsic lower thermal stability of WL fillers respect to the neat polymers. In fact, WL start their degradation at 257 °C meanwhile PA11 at 392 °C and PBS at 306 °C, as reported in Table 8. Therefore, it is reasonable to believe that in PBS-based samples also biodegradation should be favorited by using WL as filler even if degradative agents are different. This consideration is supported by other works regarding biodegradation of composites [52]. Thus, PBS-based samples with improved HDT and encouraged biodegradation could represent very useful materials for some single-use applications where heat resistance and composability are simultaneously needed, as, for instance, plastic cutlery.

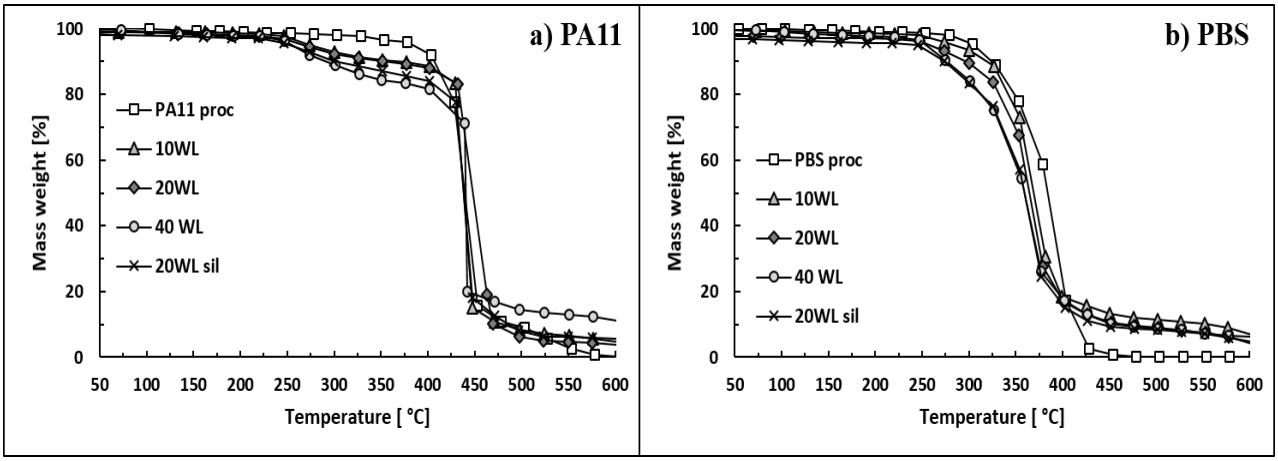

Fig.9 TGA curves of (a) PA11 and (b) PBS-based samples under air flow.

Table 8
Temperatures at 5, 10 and 15 % mass loss and residues at 600 °C for WL, PA11 and PBS-based samples.

Sample code	HDT [°C]	T_5 [°C]	T_{10} [°C]	T_{15} [°C]	Res_{600} [%]
PA11 proc	55.3	392	408	418	0.0
PA11 10 WL	61.1	284	369	425	3.9
PA11 20 WL	60.0	262	351	427	4.6
PA11 40 WL	61.6	253	289	336	11.2
PA11 20 WL sil	59.8	251	303	387	5.5
PBS proc	67.5	306	325	339	0.0
PBS 10 WL	79.5	284	321	336	4.4
PBS 20 WL	79.5	261	298	322	6.2
PBS 40 WL	78.6	257	276	297	7.1
PBS 20 WL sil	79.1	248	274	293	5.0
WL	-	257	264	267	40.0

4. Conclusions

New bio-composites formed by PA11 or PBS and WL in different contents have been processed by twin-screw extruder and injection molding machine and deeply characterized. Thermal properties have been not significantly altered by WL: only T_g values have been slightly decreased by WL particles suggesting a plasticization effect of the filler on the matrix. This aspect has been reflected in elongation at break values that have been maintained particularly high despite the significant WL loading. Tensile test has also pointed out a good WL stiffening effect (Young modulus of WL of around 2-3 GPa) and a good polymers-WL adhesion (Pukanszky's B adhesion factor of around 1.3). The WL stiffening effect have been reflected also on higher storage modulus (E') within a broad

temperature range. Moreover, a correlative prediction formula for WL filled bio-composites storage modulus has been proposed. Three different micro-mechanical models have been fitted on experimental creep test data to extent and predict the viscoelastic behavior of investigated composites. Each model has pointed out the WL ability to improve both the instantaneous elastic and the final viscous creep resistance. By the way, using WL the time needed to reach the maximum asymptotic creep compliances has been reduced if compared with neat polymers. Thermal and heat resistance of bio-composites has been smartly modified by WL. In fact, HDT has been enhanced meanwhile TGA curves have been significantly shifted to lower temperatures. Finally, reactive extrusion with silane seems to have not given special benefits to composites and alternative coupling strategies should be investigated in order to further improve their mechanical properties.

References

[1] C. Wilcox, E. Van Sebille, B.D. Hardesty, Threat of plastic pollution to seabirds is global, pervasive, and increasing, Proceedings of the National Academy of Sciences 112(38) (2015) 11899-11904.
[2] J.D. Hamilton, Understanding crude oil prices, National Bureau of Economic Research, 2008.
[3] L. Martino, L. Basilissi, H. Farina, M.A. Ortenzi, E. Zini, G. Di Silvestro, M. Scandola, Bio-based polyamide 11: Synthesis, rheology and solid-state properties of star structures, European Polymer Journal 59 (2014) 69-77.
[4] M. Niaounakis, Biopolymers: applications and trends, William Andrew2015.
[5] P. Dang, M. Werth, R. Marchioni, J. Mason, S. ATOFINA, S. Rio Claro, Thermoplastic materials in oil and gas applications: 30 years experience with polyamide 11 from offshore production to onshore distribution, (2004).
[6] H. Song, S.Y. Lee, Production of succinic acid by bacterial fermentation, Enzyme and microbial technology 39(3) (2006) 352-361.
[7] J. Zeikus, M. Jain, P. Elankovan, Biotechnology of succinic acid production and markets for derived industrial products, Applied microbiology and biotechnology 51(5) (1999) 545-552.
[8] H. Yim, R. Haselbeck, W. Niu, C. Pujol-Baxley, A. Burgard, J. Boldt, J. Khandurina, J.D. Trawick, R.E. Osterhout, R. Stephen, Metabolic engineering of Escherichia coli for direct production of 1, 4-butanediol, Nature chemical biology 7(7) (2011) 445.
[9] B.-B.B. Blocks, Polymers in the World-Capacities, Production and Applications: Status Quo and Trends Towards 2020, Nova Institute (2015).
[10] European-Bioplastics, Bioplastics market data 2018 - Global production of bioplastics 2018-2023, 2018.
[11] Plastics-Europe, Plastics the fact: an analysis of European plastics production, demand and waste data, 2018.
[12] A. Keller, Compounding and mechanical properties of biodegradable hemp fibre composites, Composites Science and Technology 63(9) (2003) 1307-1316.
[13] S. Yang, S. Bai, Q. Wang, Sustainable packaging biocomposites from polylactic acid and wheat straw: enhanced physical performance by solid state shear milling process, Composites Science and Technology 158 (2018) 34-42.

[14] A. Nanni, M. Messori, A comparative study of different winemaking by-products derived additives on oxidation stability, mechanical and thermal proprieties of polypropylene, Polymer Degradation and Stability 149 (2018) 9-18.
[15] A. Nanni, M. Messori, Effect of the wine lees wastes as cost-advantage and natural fillers on the thermal and mechanical properties of poly(3-hydroxybutyrate-co-hydroxyhexanoate) (PHBH) and poly(3-hydroxybutyrate-co-hydroxyvalerate) (PHBV), Under Submission (2019).
[16] A. Nanni, D. Battegazzore, A. Frache, M. Messori, Thermal and UV aging of polypropylene stabilized by wine seeds wastes and their extracts, Polymer Degradation and Stability Under review (2019).
[17] J.S. Choi, W.H. Park, Effect of biodegradable plasticizers on thermal and mechanical properties of poly (3-hydroxybutyrate), Polymer testing 23(4) (2004) 455-460.
[18] S.-H. Lee, S. Wang, Biodegradable polymers/bamboo fiber biocomposite with bio-based coupling agent, Composites Part A: Applied Science and Manufacturing 37(1) (2006) 80-91.
[19] C.M. Galanakis, Handbook of Grape Processing by-Products: Sustainable Solutions, Academic Press2017.
[20] OIV, The International Organisation of Vine and Wine. Available from: http://www.oiv.int/public/medias/6371/oiv-statistical-report-on-world-vitiviniculture-2018.pdf, 2018.
[21] V. Novello, Filiera vitivinicola: Valorizzare residui e sottoprodotti, Informatore Agrario 33 (2015) 61-63.
[22] G. Mago, D.M. Kalyon, F.T. Fisher, Nanocomposites of polyamide-11 and carbon nanostructures: Development of microstructure and ultimate properties following solution processing, Journal of Polymer Science Part B: Polymer Physics 49(18) (2011) 1311-1321.
[23] J. Xu, B.H. Guo, Poly (butylene succinate) and its copolymers: research, development and industrialization, Biotechnology journal 5(11) (2010) 1149-1163.
[24] W. Voigt, Ueber die Beziehung zwischen den beiden Elasticitätsconstanten isotroper Körper, Annalen der Physik 274(12) (1889) 573-587.
[25] J. Halpin, Stiffness and expansion estimates for oriented short fiber composites, Journal of Composite Materials 3(4) (1969) 732-734.
[26] B. Pukanszky, Influence of interface interaction on the ultimate tensile properties of polymer composites, Composites 21(3) (1990) 255-262.
[27] R.R. Sujan EBW, Using the DMA Q800 for ASTM International D 648 Deflection Temperature Under Load TA Instruments, 109 Lukens Drive, New Castle DE 19720, USA
[28] W. Kai, Y. He, Y. Inoue, Fast crystallization of poly (3-hydroxybutyrate) and poly (3-hydroxybutyrate-co-3-hydroxyvalerate) with talc and boron nitride as nucleating agents, Polymer international 54(5) (2005) 780-789.
[29] S.-Y. Fu, X.-Q. Feng, B. Lauke, Y.-W. Mai, Effects of particle size, particle/matrix interface adhesion and particle loading on mechanical properties of particulate–polymer composites, Composites Part B: Engineering 39(6) (2008) 933-961.
[30] M. Dekkers, D. Heikens, The effect of interfacial adhesion on the tensile behavior of polystyrene–glass-bead composites, Journal of Applied Polymer Science 28(12) (1983) 3809-3815.
[31] D. Battegazzore, S. Bocchini, J. Alongi, A. Frache, Rice husk as bio-source of silica: preparation and characterization of PLA–silica bio-composites, RSC Advances 4(97) (2014) 54703-54712.
[32] D. Battegazzore, A. Noori, A. Frache, Natural wastes as particle filler for poly (lactic acid)-based composites, Journal of Composite Materials (2018) 0021998318791316.
[33] Y.Y. Then, N.A. Ibrahim, N. Zainuddin, H. Ariffin, W.M.Z. Wan Yunus, Oil palm mesocarp fiber as new lignocellulosic material for fabrication of polymer/fiber biocomposites, International Journal of Polymer Science 2013 (2013).

[34] J. Jancar, A. Dibenedetto, Failure Mechanics in Ternary Composites of Polypropylene with Inorganic Fillers and Elastomer Inclusions. 2. Fracture-Toughness, Journal of materials science 30(9) (1995) 2438-2445.
[35] N. Sallem-Idrissi, P. Van Velthem, M. Sclavons, Fully bio-sourced Nylon 11/raw lignin composites: thermal and mechanical performances, Journal of Polymers and the Environment 26(12) (2018) 4405-4414.
[36] R. Sailaja, M. Deepthi, Mechanical and thermal properties of compatibilized composites of polyethylene and esterified lignin, Materials & Design 31(9) (2010) 4369-4379.
[37] H. Oliver-Ortega, L. Granda, F. Espinach, J. Mendez, F. Julian, P. Mutjé, Tensile properties and micromechanical analysis of stone groundwood from softwood reinforced bio-based polyamide11 composites, Composites Science and Technology 132 (2016) 123-130.
[38] C. Taesler, H. Wittich, C. Jürgens, K. Schulte, H. Kricheldorf, Polymer whiskers of poly (4-hydroxybenzoate): Reinforcement efficiency in composites with polyamides, Journal of applied polymer science 61(5) (1996) 783-792.
[39] L. Liu, J. Yu, L. Cheng, W. Qu, Mechanical properties of poly (butylene succinate)(PBS) biocomposites reinforced with surface modified jute fibre, Composites Part A: Applied Science and Manufacturing 40(5) (2009) 669-674.
[40] S. Sahoo, M. Misra, A.K. Mohanty, Enhanced properties of lignin-based biodegradable polymer composites using injection moulding process, Composites Part A: Applied Science and Manufacturing 42(11) (2011) 1710-1718.
[41] S.B. Mishra, A. Mishra, N. Kaushik, M.A. Khan, Study of performance properties of lignin-based polyblends with polyvinyl chloride, Journal of Materials Processing Technology 183(2-3) (2007) 273-276.
[42] P. Zierdt, T. Theumer, G. Kulkarni, V. Däumlich, J. Klehm, U. Hirsch, A. Weber, Sustainable wood-plastic composites from bio-based polyamide 11 and chemically modified beech fibers, Sustainable Materials and Technologies 6 (2015) 6-14.
[43] R.S. Lakes, Viscoelastic solids, CRC press1998.
[44] J. Burgers, First report on viscosity and plasticity, Nordemann Pub., New York (1935).
[45] D. Holmes, J. Loughran, H. Suehrcke, Constitutive model for large strain deformation of semicrystalline polymers, Mechanics of Time-Dependent Materials 10(4) (2006) 281-313.
[46] R.G. Palmer, D.L. Stein, E. Abrahams, P.W. Anderson, Models of hierarchically constrained dynamics for glassy relaxation, Physical Review Letters 53(10) (1984) 958.
[47] F. Bondioli, A. Dorigato, P. Fabbri, M. Messori, A. Pegoretti, Improving the creep stability of high-density polyethylene with acicular titania nanoparticles, Journal of applied polymer science 112(2) (2009) 1045-1055.
[48] K.S. Fancey, A mechanical model for creep, recovery and stress relaxation in polymeric materials, Journal of materials science 40(18) (2005) 4827-4831.
[49] W.N. Findley, 26-Year creep and recovery of poly (vinyl chloride) and polyethylene, Polymer Engineering & Science 27(8) (1987) 582-585.
[50] M.S. Huda, L.T. Drzal, A.K. Mohanty, M. Misra, Effect of fiber surface-treatments on the properties of laminated biocomposites from poly (lactic acid)(PLA) and kenaf fibers, Composites science and technology 68(2) (2008) 424-432.
[51] J. Lee, Z.M. Ishak, R.M. Taib, T. Law, M.A. Thirmizir, Mechanical, thermal and water absorption properties of kenaf-fiber-based polypropylene and poly (butylene succinate) composites, Journal of Polymers and the Environment 21(1) (2013) 293-302.
[52] N. Teramoto, K. Urata, K. Ozawa, M. Shibata, Biodegradation of aliphatic polyester composites reinforced by abaca fiber, Polymer Degradation and Stability 86(3) (2004) 401-409.